ChemComm

Accepted Manuscript

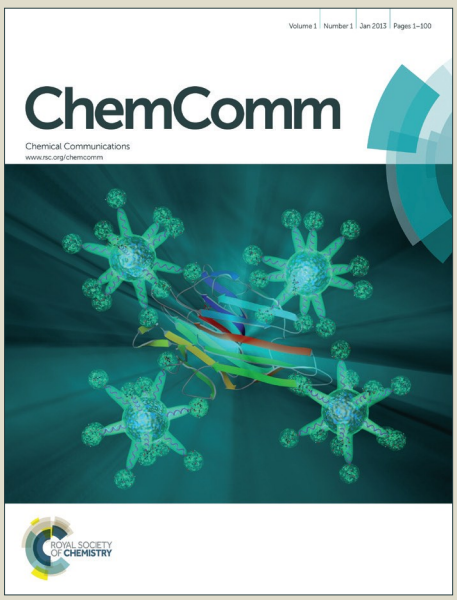

ROYAL SOCIETY OF CHEMISTRY

www.rsc.org/chemcomm

Chemical Communications

COMMUNICATION

Pharmaceutical nanocrystals confined in porous host systems - Interfacial effects and amorphous interphases

N. Sonnenberger,[a] N. Anders,[b] Y. Golitsyn,[c] M. Steinhart,[d] D. Enke,[b] K. Saalwächter,[c] and M. Beiner [a,e]

Received 31st January 2016,
Accepted 00th January 20xx

DOI: 10.1039/x0xx00000x

www.rsc.org/

DSC and NMR results prove the existence of an amorphous acetaminophen nanolayer between acetaminophen nanocrystals (form I and form III) and pore walls in controlled porous glasses. This nanolayer controls the surface energy. This finding is highly relevant for approaches towards crystal engineering in nanopores and indicates similarities to the situation during early stages of crystallization in polymorphic bulk samples.

An important requirement for pharmaceuticals is to control and stabilize their polymorphic state determining application-relevant properties like solubility or bioavailability.[1] In recent years, it has been demonstrated that confinement in nanopores can be an efficient route towards crystal engineering.[2-6] Polymorphs which are inaccessible or metastable in bulk systems have been grown and investigated in nanoporous host systems like controlled porous glass (CPG),[2-5] self-assembled polymers[2] or self-ordered nanoporous alumina[3,6,7] with typical pore diameters in the range 5-100 nm. The results obtained so far have been rationalized by thermodynamic equilibrium models[5] as well as models based on changes in nucleation behaviour and crystal growth.[6,7] However, the understanding of the physical reasons for changes in the polymorphic state in nanopores is still incomplete. Changes of the surface energy seem to be of particular interest considering thermodynamic equilibrium concepts. In this context it is very important to know whether the nanocrystals are in direct contact with the pore wall or separated by an amorphous interphase from the pore wall. Both situations have been considered in the literature.[8,9] The main aim of this letter is therefore to clarify the situation at the surface of nanocrystals confined in a nanoporous host system by a combination of calorimetric methods and solid-state NMR techniques. The crystallization behaviour of the pharmaceutical model drug acetaminophen (ACE) is investigated in CPG nanopores with hydroxyl-terminated silica at the pore walls.

Monolithic CPG membranes with pore diameters from 8 nm to 89 nm and thicknesses of about 500 µm were produced by spinodal decomposition of sodium borosilicate glass (70 w% SiO_2, 23w% B_2O_3, 7 w% Na_2O) followed by leaching steps.[10] The resulting CPG membranes with narrow pore size distribution and porosities in the range from 40 to 64% (cf. ESI, Table A1) were dried under vacuum at 180°C for two hours before filling. Afterwards, the CPG membranes were infiltrated by immersing them in molten ACE (Sigma Aldrich, CAS: 103-90-2) at 180 °C. The mass of the guest system was determined based on the weights of the empty CPG membrane and the filled membrane after careful cleaning of the outer surfaces with a scalpel. The pores are practically completely filled with ACE (cf. ESI, Table A1).

The dependence of melting temperature T_m and melting enthalpy ΔH_m on pore size d_p was determined based on classical DSC experiments on differently treated samples containing ACE in two different polymorphic states.[3] Form I nanocrystals occur within the pores if CPG membranes are cooled directly after filling in the presence of a bulk ACE layer on top of the membranes which contains heterogeneous nuclei (procedure (i)). Form III is growing during isothermal (cold) crystallization at T_c = 80°C for 2h after reheating the cleaned CPG membranes (without bulk ACE layer) to 180°C, quenching it to the glassy state and bringing it back to T_c (procedure (ii); cf. inset Figure 1). The aim of both procedures is to obtain pure polymorphs of ACE and to reach a maximum degree of crystallinity of the confined pharmaceuticals. This allows to study changes of ΔH_m depending on pore diameter d_p and crystal size d_c.

Typical DSC heating scans (+10 K/min) for filled CPG membranes with different pore diameters d_p crystallized according to procedure (i) and measured without bulk ACE on top are shown as full lines in Figure 1. Two melting peaks are observed. The peak at higher temperatures corresponds to residues of bulk ACE on the outer surfaces. This material melts at the bulk melting temperature of the monoclinic form I of ACE ($T_{m,I}^{\infty}$ = 167-169°C)[3,11] independent of d_p.

[a] Martin-Luther-Universität Halle-Wittenberg, Naturwissenschaftliche Fakultät II, Institut für Chemie, Heinrich-Damerow-Str. 4, 06120 Halle (Saale), Germany.
[b] Universität Leipzig, Institut für Technische Chemie, Lineestr. 3-4, 04103 Leipzig, Germany.
[c] Martin-Luther-Universität Halle-Wittenberg, Naturwissenschaftliche Fakultät II, Institut für Physik, Betty-Heimann-Str. 3, 06120 Halle (Saale), Germany.
[d] Universität Osnabrück, Institut für Chemie neuer Materialien, Barbarastr. 7, 49076 Osnabrück, Germany.
[e] Fraunhofer-Institut für Mikrostruktur von Werkstoffen und Systemen IMWS, Walter-Hülse-Str. 1, 06120 Halle (Saale), Germany.

Electronic Supplementary Information (ESI) available: Details about the properties of the controlled porous glasses used and the thermodynamic parameters of ACE nanocrystals in pores with different diameters are given in the supplementary information. See DOI: 10.1039/x0xx00000x

The main melting peak, however, is located at lower temperatures and originates from ACE in nanopores. As expected,[3,8] this peak shifts with decreasing pore size significantly towards lower temperatures in accordance with the Gibbs-Thomson equation. Moreover, there is a decrease of the main peak area ($\Delta H_{m,I}$ calculated per gram ACE) with decreasing pore diameter as reported in the literature for other host-guest systems.[8,12-16]

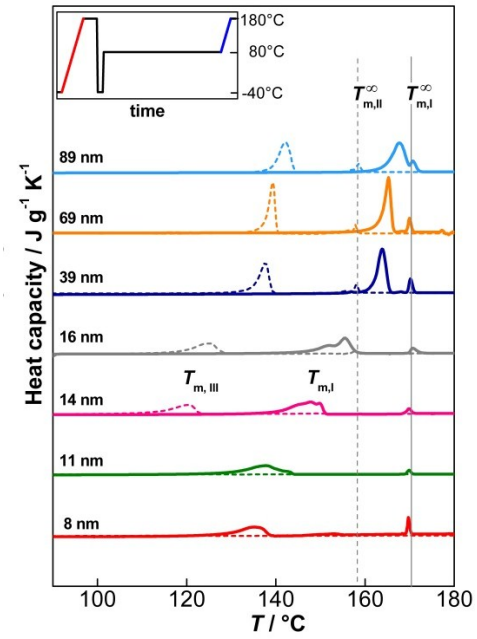

Figure 1. DSC heating scans for ACE confined in CPGs with different pore sizes prepared following procedure (i) [solid lines] or procedure (ii) [dashed lines]. Curves are vertically shifted by 20 Jg^{-1}K^{-1}. The inset shows the applied temperature program where the first scan (red) represents procedure (i), while the second scan (blue) corresponds to procedure (ii) as described in the main text.

The dashed lines in Figure 1 indicate DSC heating scans (+10 K/min) for samples which are cold-crystallized at T_c = 80°C according to procedure (ii). The main melting peak occurs in this case generally at much lower temperatures (120-140°C) and shifts again systematically to lower temperatures with decreasing pore diameter d_c. The consistently reduced melting temperatures indicate the formation the commonly inaccessible form III of ACE during isothermal crystallization at low T_c, as reported previously.[3,5] The $\Delta H_{m,III}$ values per gram ACE taken from the main melting peak tend to decrease with decreasing d_p. Note that it has been shown for ACE that the $\Delta H_{m,III}$ is practically constant after 2h annealing at T_c for pore diameters $d_p \geq 14$ nm and that form III grows in pores with $d_p \leq 11$ nm only after an additional nucleation step (cf. ESI, Table A2).

Plotting the melting temperatures of form I and form III, $T_{m,I}$ and $T_{m,I}$, as function of inverse pore diameter d_p^{-1} (full symbols in Figure 2) a nearly linear dependence is observed in accordance with the Gibbs-Thomson equation

$$T_m(d_c) = T_m^{\infty} \cdot \left(1 - \frac{4 \cdot \sigma_{cl}}{d_c \cdot \Delta H_m^{\infty} \cdot \rho_c}\right) \quad (1)$$

with σ_{cl} being the relevant specific surface energy, d_c the diameter of cylindrical nanocrystals and ρ_c being the density of the crystal. Assuming that d_c is equal to the pore diameter d_p, $\rho_{c,I}$ = 1.293 g/cm³ and $\Delta H_{m,I}$ = 185.9 J/g [3,11] one gets $\sigma_{cl,I}$ = 0.0437 J/m^2 as specific surface energy of form I.

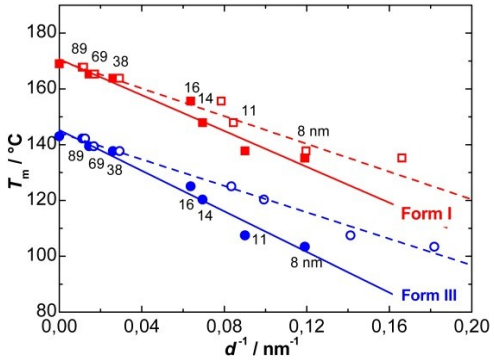

Figure 2. Gibbs-Thomson plots for ACE nanocrystals of form I (squares) and form III (circles) grown in CPGs with different pore diameters. In case of the full symbols the pore diameter d_p is considered as relevant diameter while the crystal size $d_c = d_p - 2l_a$ is considered in case of the open symbols. Solid and dashed lines correspond to Gibbs-Thomson fits to full and open symbols, respectively.

A main part of this study was the evaluation of the dependence of ΔH_m on the pore diameter d_p. Diameter-dependent values for the heats of melting, $\Delta H_{m,I}$ and $\Delta H_{m,III}$, are taken from DSC heating scans for differently prepared samples considering only the main melting peak, i.e., ACE located in nanopores. Both values, $\Delta H_{m,I}$ and $\Delta H_{m,III}$, decrease systematically with deceasing pore diameter and differ from the bulk values for $\Delta H_{m,I}^{\infty}$ and $\Delta H_{m,III}^{\infty}$ = 165 ± 15 J/g reported in the literature.[3] Considering a two phase model with an amorphous ACE layer on the pore walls,[8,9,12-16] this observation corresponds to a significant reduction of the degree of crystallinity calculated from $f_c = \Delta H_m / \Delta H_m^{\infty}$. Typical thicknesses reported in such cases are in the range 1-3 nm. An amorphous ACE layer located between pore wall and confined nanocrystal may occur due to strong interaction between pore wall and host system preventing crystallization at the interface. For nanocrystals in cylindrical pores one gets a simple equation predicting the dependence of ΔH_m on the pore diameter d_p

$$\Delta H_m(d_p) = \Delta H_m^{\infty} \cdot \left(1 - \frac{2l_a}{d_p}\right)^2 \quad (2)$$

where ΔH_m^{∞} is the heat of melting for bulk-like crystals, l_a is the thickness of an amorphous layer located at the pore walls and $d_c = d_p - 2l_a$ is the diameter of the nanocrystals.

In Figure 3a experimental values for $f_c \cdot d_p^2$ are plotted as function of pore diameter d_p for forms I and III of ACE in CPGs together with fits based on Eq.(2). Obviously, the data are approximated quite well if an average thickness of the amorphous, non-crystallizable layers of $l_{a,I}$ = 2.14 nm and $l_{a,III}$ = 2.70 nm are used for form I and III, respectively. The amorphous layer thickness can be also determined based on Eq.(2) for each pore diameter independently (cf. ESI, Table A2). The average values from these calculations ($l_{a,I}$ = 2.14 nm; $l_{a,III}$ = 2.71 nm) agree well with the l_a values from the fits in Figure 3a. Note that one has also to use the nanocrystal diameters (d_c) instead of d_p in Figure 2 if this model is correct. This results in smaller surface energy values of $\sigma_{cl,I}$ = 0.0338 J/m^2 for form I as compared to $\sigma_{cl,I}$ = 0.0437 J/m^2 without this correction.

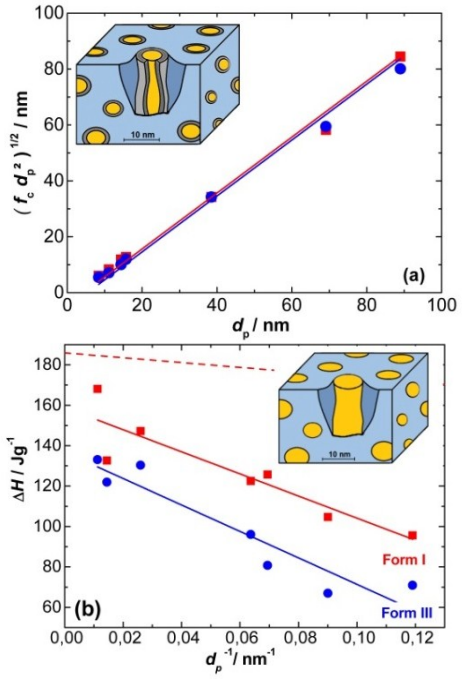

Figure 3. (a) $f_c \cdot d_p^2$ *vs*. pore diameter d_p as well as (b) ΔH_m *vs*. d_p^{-1} for form I (squares) and form III (circles) of ACE in nanopores. The full lines in part (a) are fits based on Eq.(2) and the full lines in part (b) are free fits based on Eq.(3). The dashed line in part (b) is the prediction of Eq.(3) using the pre-factor determined for form I based on Eq.(1) and Figure 2 as well as $\Delta H_{m,I}^{\infty}$ = 185,9 J/g. The insets show sketches of the considered situations.

Although Eq.(2) seems to work quite well, we have also to consider alternative approaches explaining the ΔH_m reduction in nanopores without assuming an amorphous layer. Thermodynamic models considering the influence of the increased surface energy in nanocrystals on the melting enthalpy[8,9,17,18] predict an entirely different dependence of ΔH_m on the diameter d_c

$$\Delta H_m(d_c) = \Delta H_m^{\infty} - \frac{4\,\sigma_{cl}}{\rho_c \cdot d_c}. \qquad (3)$$

The diameter of the nanocrystal d_c would correspond in this homogenous model exactly to the pore diameter d_p. In accordance with Eq.(3), $\Delta H_{m,I}$ and $\Delta H_{m,III}$ are plotted *vs*. inverse pore diameter d_p^{-1} in Figure 3b. The solid lines are free fits to the experimental data based on Eq.(3). Note that the extrapolation to $d_p^{-1} = 0$ gives values of 158.8 J/g and 136.8 J/g which are significantly smaller than $\Delta H_{m,I}^{\infty}$ and $\Delta H_{m,III}^{\infty}$. The pre-factors $4\sigma_{cl}/\rho_c$ are $5.47 \cdot 10^{-7}$ Jm/g and $6.55 \cdot 10^{-7}$ Jm/g for form I and form III, respectively. These $4\sigma_{cl}/\rho_c$ values are obviously much larger than those which are obtained from the T_m vs. d_p^{-1} plot in Figure 2. The dashed line in Figure 3b is a prediction of Eq.(2) if the experimentally obtained pre-factor $4\sigma_{cl,I}/(\rho_{c,I}\ \Delta H_{m,I}^{\infty})$ from Figure 2 is used and $\Delta H_{m,I}^{\infty}$ = 185,9 J/g is assumed to be a constant. Obviously, this prediction cannot describe the experimentally detected dependence of ΔH_m on the inverse pore diameter. Altogether the comparisons made here clearly indicate the existence of an amorphous interphase for the investigated host guest systems.

From a thermodynamic point of view a major difference between the two approaches discussed above is that Eq.(2) considers an amorphous ACE layer located between pore wall and nanocrystal while in Eq.(3) the crystals are assumed to be in direct contact with the pore wall. Depending on the situation the surface energy considerations have to be different and the requirements regarding a rational crystal design will be influenced.[5] From that perspective it is very important to know the fundamental reasons for the observed reduction in ΔH_m and whether or not the heterogeneous model is relevant. Hence, additional solid-state NMR measurements were performed on CPGs containing ACE in order to directly probe the possible existence of an amorphous ACE interphase.

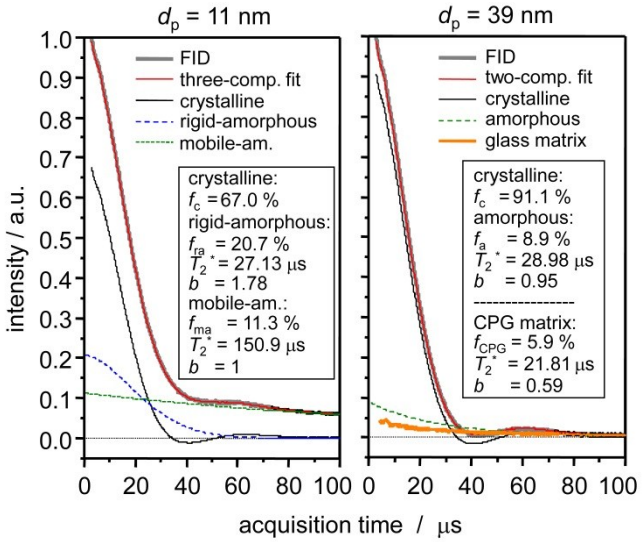

Figure 4. Static ^{1}H NMR free-induction decays recorded at 200 MHz Larmor frequency and 100°C for ACE in CPG with d_p of 11 nm (left) and 39 nm (right), including component decompositions as described in the text. The fitting parameters are given in the insets. We have used a Bruker Avance III instrument with a dedicated static probehead featuring a short dead time of only 2.5 µs and a 90° pulse length of the same order.

Following previously published procedures,[19] we measured ^{1}H free-induction decay (FID) data on two different filled (as well as the unfilled ones as reference for the background signal), and used lineshape decomposition to determine quantitatively the ^{1}H signal fractions associated with crystalline and amorphous CPG (Figure 4). The method is based upon the fact that the apparent transverse relaxation time (T_2^*) of the FID signal, and its actual shape, is governed by multiple strong dipole-dipole couplings among the many protons. T_2^* is shortest for the rigid crystalline fraction, and longer for an amorphous component that is characterized by a lower density (thus lower couplings). Enhanced local mobility, which also prolongs T_2^* and changes the signal shape if the associated correlation time of motion is faster than around 10 µs, can also have an effect. As the FID of the pure crystal (measured on bulk ACE) could not be fitted with commonly used signal functions,[19] our fits of the filled-CPG data were thus based upon the use of smoothed and interpolated experimental data taken on bulk crystalline ACE at the same temperature, plus one or two additional components modelled by modified (stretched or compressed) exponentials, $f \cdot \exp\{-(t/T_2^*)^b\}$.[19] Unlike the simpler case of semi-crystalline polymers,[19] where the amorphous phase can be highly mobile (T_2^* in the ms range) and more easily separable, we here observed an only moderately increased amorphous T_2^* in the studied temperature range between 40 and 100°C. In this range, the results reported below did not change significantly.

In the 11 nm sample we found two additional signal fractions with T_2^* of around 30 and 150 μs, tentatively denoted as rigid-amorphous and mobile-amorphous, respectively. We also considered the background signal associated with CPG (mainly surface-related –OH and H_2O), as determined by measurements on identical amounts of empty CPG with identical thermal treatment. In both cases, it amounted to around 5% of the total signal (shown only in the right panel of Figure 4), featuring a T_2^* of around 30 μs. It thus contributes to the rigid-amorphous component in the filled CPG. Thus, the mobile-amorphous fraction consists of ACE. We anticipate that due to an easier re-uptake of H_2O, the measurement of the empty CPG may well result in overestimated background signal, thus providing an upper limit.

In the 39 nm sample we found a significantly reduced amorphous component, with even negligible mobile-amorphous fraction. Based upon the fractions given in the insets of Figure 4 and a cylindrical-core-shell model with crystalline core and an amorphous shell, and excluding a hydrated background layer, we estimate a total amorphous layer thickness of 0.86 nm and 0.4 nm for the 11 nm and 39 nm pores, respectively. While the agreement with the DSC-based estimates (1.37 and 2.13 nm, resp.) is satisfactory in the former case, we think that the larger deviation in the latter case might be at least partly due to the possibly overestimated background and uncertainties in the procedure, which become larger at the given rather low amorphous content.

In summary, the results of the presented DSC and NMR experiments on CPGs filled with ACE evidence the existence of an amorphous ACE fraction which is most likely located at the CPG pore walls in accordance with the amorphous layer model.[11] The thickness of this interphase calculated based on NMR data is somewhat smaller than the l_a values calculated from calorimetric data using Eq.(2). Despite the remaining differences regarding the layer thickness, both experimental methods, DSC and NMR, strongly support the existence of an amorphous interphase, i.e. a non-crystallizable ACE nanolayer between hydroxyl-terminated silica pore wall and ACE nanocrystals in CPG pores. Similar behaviour has been also found for CPGs filled with ibuprofen where l_a values of about 1-3 nm have been observed.[20] Although effects due to a minimization of the curved crystal surface area according to Eq.(3) are not fully excluded, the influence of the amorphous interphase seems to be most important for the reduction of ΔH_m in nanopores. In particular, there seem to be clear evidences supporting the assumption that the surfaces of pharmaceutical nanocrystals in the investigated host-guest systems are commonly not in direct contact with the hydroxyl-terminated silica pore walls but surrounded by an amorphous ACE nanolayer. Consequently, the thermodynamically relevant surface energy is that between crystalline and amorphous ACE. Accordingly, the overall situation in our host-guest-systems should be comparable to early stages of crystallization where isolated nanocrystals are formed in the melt,[21] although the amorphous ACE interphase on the pore walls might be immobilized and slightly differently packed compared to an ordinary melt.[22] Surface modifications of the CPG pore walls do not directly influence the surface of the ACE crystals as long as the amorphous ACE interphase occurs. This applies even though it is reasonable to assume that the nature of the ACE interphase might be slightly altered by modified pore walls. This is important for crystal engineering approaches aimed to control the polymorphic state of pharmaceuticals and confirms that studies on confined nanocrystals allow to study early stages of crystallization experimentally which are usually unexplored in bulk systems since related nanocrystals are rare and occur randomly in space and time.

The authors acknowledge financial support by the DFG (Grant numbers BE 2352/4, EN 942/1, STE 1127/14 and SFB/TRR 102).

Notes and references

1 J. Bernstein, *Polymorphism in molecular crystals*, Oxford Science Publications, 2007.
2 J.-M. Ha, J. H. Wolf, M. A. Hillmyer and M. D. Ward, *J. Am. Chem. Soc.*, 2004, **126**, 3382-3383; J.-M. Ha, M. A. Hillmyer and M. D. Ward, *J. Phys. Chem. B,* 2005, **109**, 1392-1399.
3 M. Beiner, G. T. Rengarajan, S. Pankaj, D. Enke and M. Steinhart, *Nano Lett.* 2007, **7**, 1381-1385.
4 J.-M. Ha, B. D. Hamilton, M. A. Hillmyer and M. D. Ward, *Cryst. Growth Des.,* 2009, **9**, 4766-4777; B. D. Hamilton, J.-M. Ha, M. A. Hillmyer and M. D. Ward, *Acc. Chem. Res*., 2012, **45**, 414–423.
5 G. T. Rengarajan, D. Enke, M. Steinhart and M. Beiner, *Phys. Chem. Chem. Phys*. 2011, **13**, 21367-21374.
6 G. Graubner, G. T. Rengarajan, N. Anders, N. Sonnenberger, D. Enke, M. Beiner and M. Steinhart, *Cryst. Growth Des.* 2014, **14**, 78–86.
7 M. Steinhart, P. Göring, H. Dernaika, M. Prabhukaran, U. Gösele, E. Hempel and T. Thurn-Albrecht, Phys. Rev. Lett. 2006, **97**, 027801.
8 C. L. Jackson and G. B. McKenna, *Chem. Mater.,* 1996, **8**, 2128–2137; M. Alcoutlabi and G.B. McKenna, *J. Phys. Condens. Matter,* 2005, **17**, R461-R524.
9 J. Sun and S. L. Simon, *Thermochim. Acta,* 2007, **463**, 32-40.
10 F. Janowski and D. Enke, Porous Glasses, in: F. Schüth, K. S. W. Sing, J. Weitkamp (Eds.), Handbook of Porous Solids, Vol. 3, Wiley-VCH, Weinheim, **2002**, p. 1432–1542.
11 A. Burger and R. Ramberger, *Mikrochem. Acta*., 1979, **II**, 273-316.
12 C. Alba-Simionesco, B. Coasne, G. Dosseh, G. Dudziak, K. E . Gubbins, R. Radhakrishnan and M. Sliwinska-Bartkowiak, *J. Phys. Condens. Matter,* 2006, **18**, R15-R68.
13 X. Di, B. Xu and G.B. McKenna, *J. Them. Anal. Calorim.,* 2013, **113**, 533-537.
14 S. Jähnert, F. Vaca Chavez, G.E. Schaumann, A. Schreiber, M. Schönhoff, and G.H. Findenegg, *Phys. Chem. Chem. Phys.,* 2008, **10**, 6039–6051.
15 G. T. Rengarajan, D. Enke, M. Steinhart and M. Beiner, *J. Mater. Chem.*, 2008, **18**, 2537-2539.
16 J. Riikonen, E. Mäkilä, J. Salonen and V.-P. Letho, *Langmuir*, 2009, **25**, 6137- 6142.
17 R. Defay and I. Prigogine, *Surface Tension and Adsorption*, John Wiley and Sons Inc., New York, **1967**.
18 J.-H. Shin, J.-Y. Parlange and M.R. Deinert, *J. Phys. Chem.*, 2013**, 139**, 044701.
19 K. Schäler, M. Roos, P. Micke, Y. Golitsyn, A. Seidlitz, T. Thurn-Albrecht, H. Schneider and K. Saalwächter, *Solid State Nucl. Magn. Reson.,* 2015, **72**, 50-63.
20 N. Sonnenberger, unpublished results
21 P. G. Debenedetti, *Nature*, 2006, **441**, 168-169.
22 Studies on untreated CPG containing amorphous salol show that an interfacial layer with a thickness of a few nanometer has a higher T_g: M. Arndt, R. Stannarius, W. Gorbatschow and F. Kremer, Phys. Rev. E, 1996, **54**, 5377- 5390. Similar behaviour is indicated for ACE in CPGs with d_p<10 nm.[15]